The effects of electron cyclotron heating and current drive on toroidal Alfvén eigenmodes in tokamak plasmas

S E Sharapov[1], M Garcia-Munoz[2], M A Van Zeeland[3], B Bobkov[4], I G J Classen[5], J Ferreira[6], A Figueiredo[6], M Fitzgerald[1], J Galdon-Quiroga[2], D Gallart[7], B Geiger[4], J Gonzalez-Martin[2], T Johnson[8], P Lauber[4], M Mantsinen[7,9], F Nabais[6], V Nikolaeva[4], M Rodriguez-Ramos[2], L Sanchis-Sanchez[2], P A Schneider[4], A Snicker[10], P Vallejos[8], and the AUG Team and the EUROfusion MST1 Team*

[1]CCFE, Culham Science Centre, Abingdon, Oxfordshire, UK
[2]FAMN Department, Faculty of Physics, University of Seville, Seville, Spain
[3]General Atomics, PO Box 85608, San Diego, USA
[4]Max Planck Institute fur Plasmaphysik, Garching, Germany
[5]FOM-Institute DIFFER, Nieuwegein, The Netherlands
[6]Instituto de Plasmas e Fusão Nuclear, Instituto Superior Técnico, Portugal
[7]Barcelona Supercomputing Center (BSC), Barcelona, Spain
[8]VR / Royal Institute of Technology KTH, Sweden
[9]ICREA, Barcelona, Spain
[10]Aalto University, Aalto, Finland
*H. Meyer et al., Nuclear Fusion FEC 2016 Special Issue (2017)
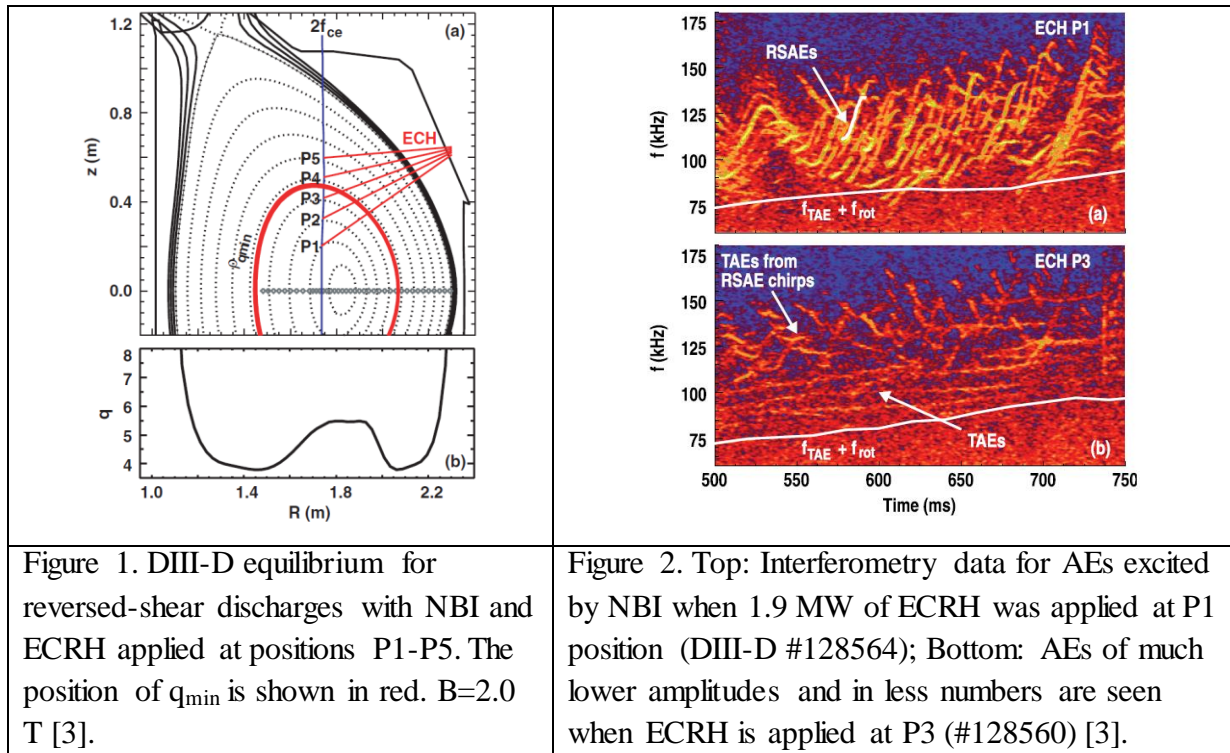
E-mail: Sergei.Sharapov@ukaea.uk

Abstract. The possibility of controlling Alfvén eigenmodes (AEs) using tools other than energetic ions is one of the most interesting and potentially important problems in the physics of burning plasmas. It has been found on DIII-D and confirmed on ASDEX-Upgrade (AUG) that electron cyclotron resonance heating (ECRH) has a profound effect on Alfvén cascades, suppressing these modes in reversed-shear plasmas. Similar studies performed for Toroidal AEs (TAEs) in AUG discharges with monotonic q-profiles have shown that ECRH can make TAEs more unstable. In these AUG discharges, energetic ions driving TAEs were obtained by ion cyclotron resonance heating. It was found that off-axis ECRH facilitated TAE instability, with TAEs appearing and disappearing on timescales of a few milliseconds when the ECRH power was switched on and off. On-axis ECRH had a much weaker effect on TAEs, and in AUG discharges performed with co- and counter-current electron cyclotron current drive (ECCD), the effects of ECCD were found to be similar to those of ECRH. Detailed TAE stability calculations have been carried out with the CASTOR-K, HAGIS, and LIGKA codes using fast ion distributions computed with the PION and SELFO codes. A significant increase in T_e caused by ECRH applied off-axis is found to increase the fast ion slowing down time and fast ion pressure causing a significant increase in the TAE drive by ICRH-accelerated ions. The rise in T_e causes also an increase in TAE radiative damping and thermal ion Landau damping, but to a lesser extent than the fast ion drive. As a result of the competition between larger drive and damping effects caused by ECRH, TAEs become more unstable.

1. Introduction

Good confinement of energetic ions produced by Neutral Beam Injection (NBI), Ion Cyclotron Resonance Heating (ICRH), and fusion-born alpha-particles during the slowing

down times is a crucial requirement for ITER plasma operations in burning plasma regimes [1, 2]. Since the energetic particle populations on ITER are super-Alfvénic and their velocities V_α satisfy $V_{Ti} << V_\alpha \approx V_A << V_{Te}$, resonant interaction between energetic particles and weakly-damped Alfvén Eigenmodes (AEs) may drive AEs unstable. If the amplitudes of AEs become high enough, a significant increase in the radial transport of the resonant energetic ions could affect significantly the power deposition profiles and increase fast ion loss to the first wall [1,2].

Possible suppression/ control of Alfvén instabilities using tools other than energetic particles is a potentially important new research avenue for burning plasmas, which started a decade ago from observation of mitigation of AEs with ECRH on the DIII-D tokamak [3]. Figure 1 shows the cross-section and safety factor q(r) in the representative reconstructed equilibria of DIII-D with NBI and ECRH applied shot-by-shot from the plasma centre (position P1) to outside the q_{min} surface (position P5). Figure 2 shows that high amplitude multiple AEs were excited by NBI when 1.9 MW of ECRH was applied close to the magnetic axis, while the AE amplitudes and the number of unstable modes were much smaller when ECRH was applied at the position of q_{min}.

Figure 1. DIII-D equilibrium for reversed-shear discharges with NBI and ECRH applied at positions P1-P5. The position of q_{min} is shown in red. B=2.0 T [3].	Figure 2. Top: Interferometry data for AEs excited by NBI when 1.9 MW of ECRH was applied at P1 position (DIII-D #128564); Bottom: AEs of much lower amplitudes and in less numbers are seen when ECRH is applied at P3 (#128560) [3].

The observed mitigation of AEs with ECRH is of great interest as ECRH is foreseen as one of the main heating and current drive techniques in ITER, even though ECRH usually does not affect strongly fast ions. Two questions were addressed following the observations [3]: i) is the ECRH suppression mechanism on AEs reproducible on other machines, and ii) what is the physics behind this effect. To answer the first question, dedicated experiments were performed on the ASDEX-Upgrade (AUG) tokamak in 2014 [4]. A technique consisting of scanning ECRH positions q_{min} (zero magnetic shear) region was employed, similar to that for DIII-D, and the ECRH suppression effect on AEs was confirmed. Moreover, a complete

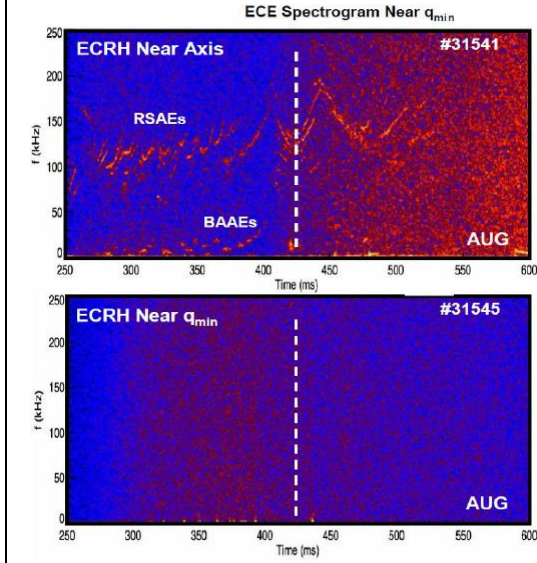suppression of AEs with ECRH applied at q_{min} was achieved in these AUG experiments as Figure 3 demonstrates.

Figure 3. ECE data on AEs excited in two AUG discharges with ECRH applied near magnetic axis (top) and near q_{min} (bottom) [4]. .
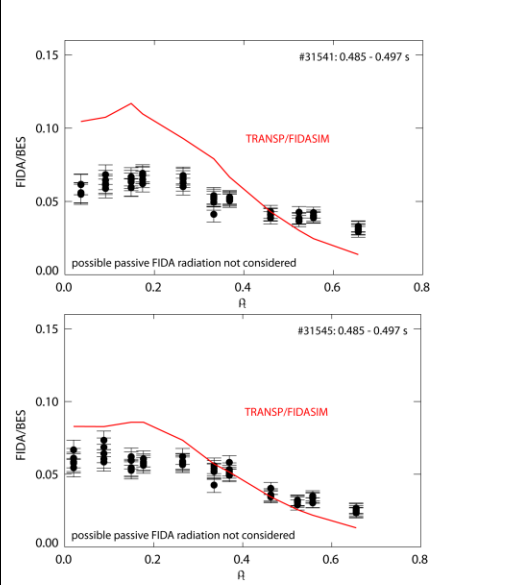
Figure 4. Radial profiles of NBI ions measured with the fast ion D_α (FIDA) diagnostics and computed with the TRANSP code in the two comparison discharges.

A comparison between the TRANSP [5] calculation for classical slowing-down of beam ions and the FIDA [6] measurements of the beam ions in the two comparison discharges shows that a classical beam distribution was obtained in the AUG discharges without AEs. In the discharge with AEs, a difference of up to ~ 30% was seen for the fast ions in the plasma core as Figure 4 shows.

The interpretation of the observed effect of ECRH suppressing AEs requires a more specific identification of the AEs suppressed. These modes associated with reversed-shear discharges were first investigated in detail on JET, where they were called Alfvén Cascade (AC) eigenmodes [7,8], and later became known as reversed-shear AEs (RSAEs) on DIII-D [3]. In contrast to the well-known TAE modes [9], the ACs are associated with the existence of q_{min} away from the magnetic axis, are localised in the vicinity of q_{min}, and their frequency f_{AC} tracks the evolution of $q_{min}(t)$ in accordance with the expression

$$2\pi f_{AC} = \left| \frac{m}{q_{min}(t)} - n \right| \cdot \frac{V_A}{R_0} + \Delta f , \qquad (1)$$

where m, n are poloidal and toroidal mode numbers, R_0 is the major radius, and Δf includes effects associated with thermal plasma pressure and pressure gradient. The frequencies of ACs lie in the band between the Geodesic Acoustic Mode (GAM) and TAE frequencies,

$$f_{GAM} \cong \frac{1}{2\pi} \left[\frac{2}{M_i R_0^2} \left(T_e + \frac{7}{4} T_i \right) \right]^{1/2} \leq f_{AC} \leq f_{TAE} \cong \frac{V_A}{4\pi q R_0} , \qquad (2)$$

where M_i is ion mass, T_e and T_i are electron and ion temperatures.

It was found as a result of additional dedicated experiments on DIII-D that with ECRH applied in the vicinity of q_{min} the electron temperature increases up to the point when GAM frequency becomes comparable to the TAE frequency, which is rather low in DIII-D discharges with q_{min} ~ 2-4. In this way, the frequency band for AC existence shrinks, and ACs are suppressed due to higher ion Landau damping associated with the acoustic oscillations [10].

This effect of the shrinking mode frequency band cannot, however, be applied to TAEs, and so the search for ECRH/ECCD effects on TAEs requires consideration of some other possibilities. Early observations on DIII-D did indicate that ECRH could also interact with TAEs [11], but more extended data were required for investigating such possibility.

2. The AUG experiment on ECRH effects on TAEs

To study ECRH/ECCD effects on TAE, discharges with monotonic q(r)-profiles and TAEs existing for long time were developed on AUG. Since it is more difficult to excite TAEs with NBI in AUG flat top plasmas with high currents $I_P > 500$ kA, ICRH-accelerated ions were employed for TAE excitation. To use hydrogen minority ICRH on the magnetic axis meant that a magnetic field of B=2.446 T was required, with plasma currents at the flat top of $I_P = 0.8$ MA. A correct choice of plasma density was one of the main issues in the experiment as the density should be neither too low (for avoiding supra-thermal electrons) nor too high (for facilitating ICRH tail of fast ions resonating with TAEs). The range of $ne(0) \approx 3 - 4.5 \times 10^{19}$ m^{-3} was chosen as an optimal one. For the ICRH power levels required, the AUG discharges were in the H-mode, and the additional use of ECRH increased plasma density in these AUG discharges by $\approx 20\%$, in a broad agreement with the interplay between ECRH and plasma density described in [12] .

2.1 Facilitation of TAE instability with ECRH applied off-axis

Figure 5 shows typical observation of ICRH-driven TAEs in the dedicated AUG discharge with ECRH modulated power 200 ms on / 200 ms off applied at normalized radius $\rho_p \approx 0.3$. Here, $\rho_p = (\psi/\psi(a))^{1/2}$ is a radial coordinate determined by the poloidal flux ψ. TAEs are excited throughout the whole discharge from ~0.5 s to ~5.5 s. Significant changes in TAEs are seen in correlation with the ECRH modulation, together with large changes in plasma density and temperature. Figure 6 shows that TAEs with toroidal mode numbers from n=2 to n=6 were excited in the frequency range 125 kHz $< f_{TAE} < 230$ kHz. The frequency sweeping of TAEs is associated with the density increase during the ECRH and the corresponding decrease in Alfvén velocity $V_A \propto B/n^{1/2}$. . Finally, Figure 7 shows that TAEs become unstable when ECRH is applied off-axis, and disappear after ECRH is switched off. A remarkably short time scale of few ms is observed in the correlation between ECRH on/off and TAE appearance/ disappearance. A similar effect on TAEs was observed with ECRH applied at larger radius of $\rho_p \approx 0.5$.

Internal measurements of the TAE mode structure were performed in the AUG discharges with reflectometry [13] and ECE imaging (ECEI) [14] diagnostics covering the mid-radius plasma region as Figure 8 shows. For TAE observed in discharge #33145 at ~ 1 s, the ECEI measurements showed that the TAE mode structure is peaked at R~1.85-1.9 m corresponding to the mid-radius, in a robust agreement with the computed TAE shown in Figure 8.
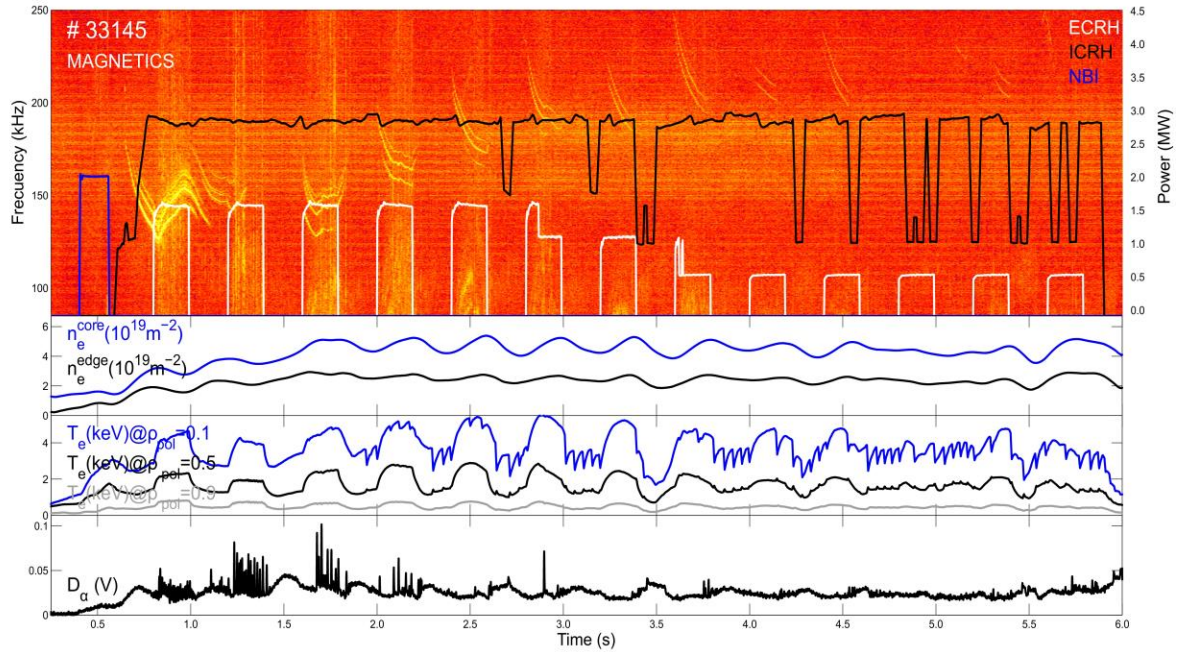

Figure 5 (colour online): From top to bottom: i) Magnetic spectrogram showing excitation of TAEs and power wave-forms of ICRH (black), ECRH (white) and NBI (blue); ii) temporal evolution of n_e on-axis and at the plasma edge, iii) temporal evolution of T_e on-axis, at half-radius, and at the plasma edge, and iv) D_α signal. AUG discharge #33145 with ECRH at r/a=0.3.
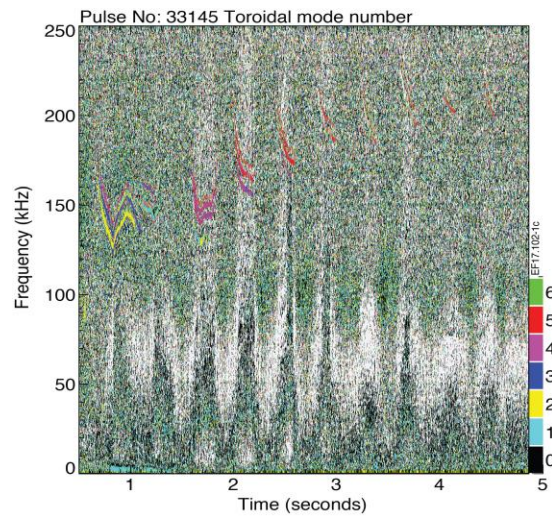
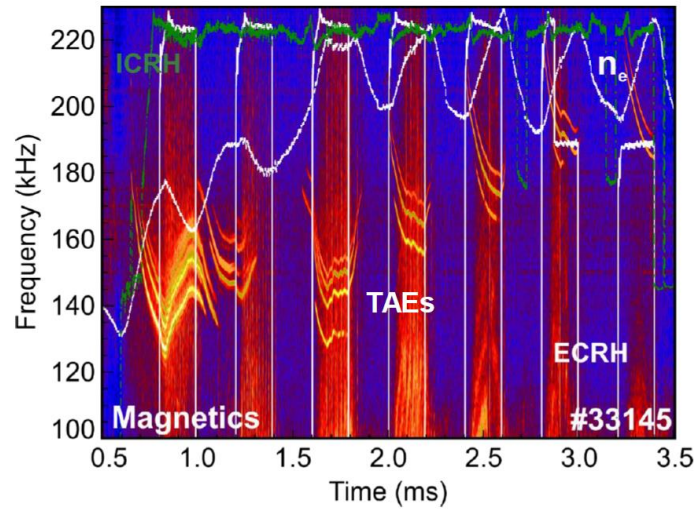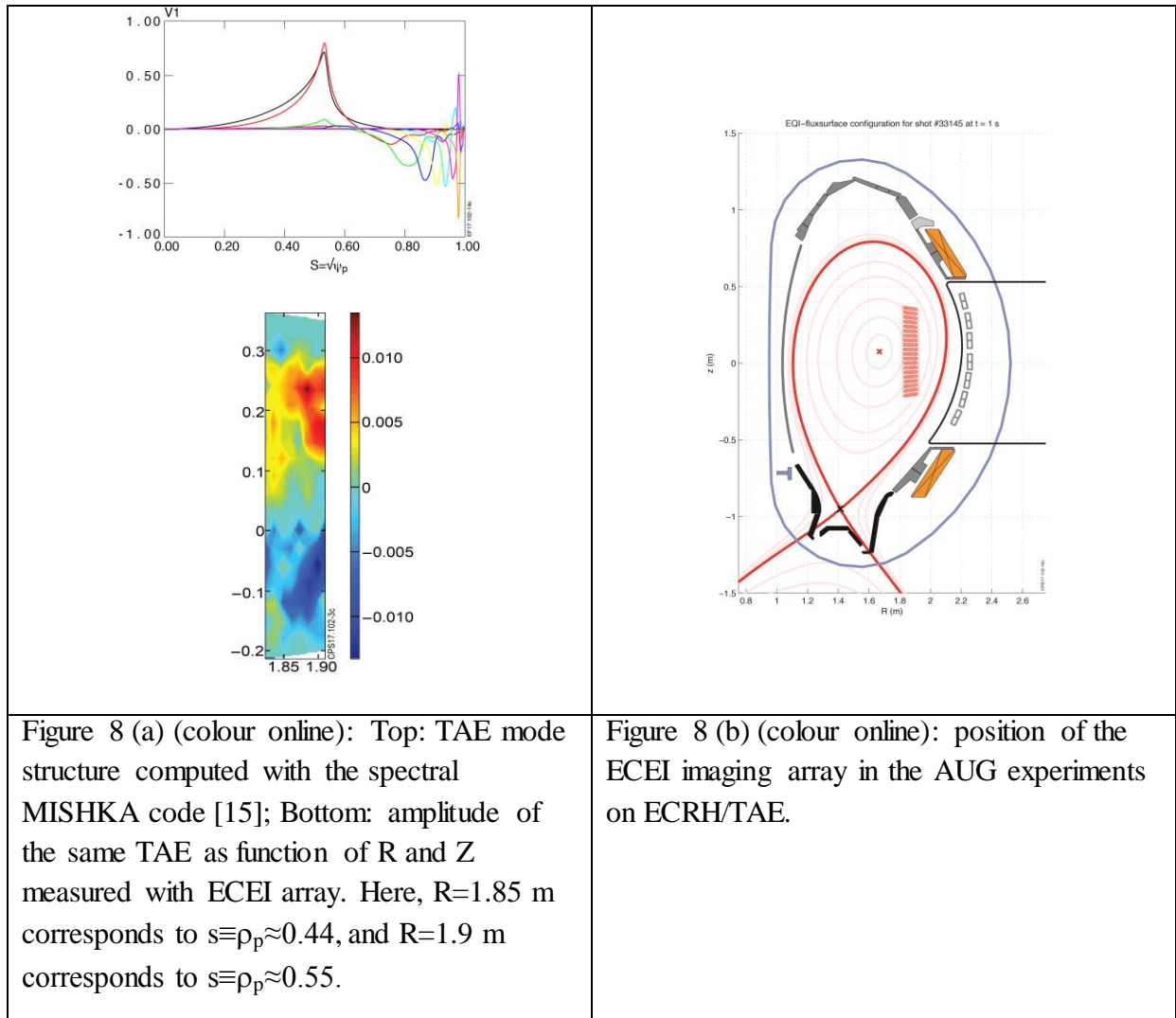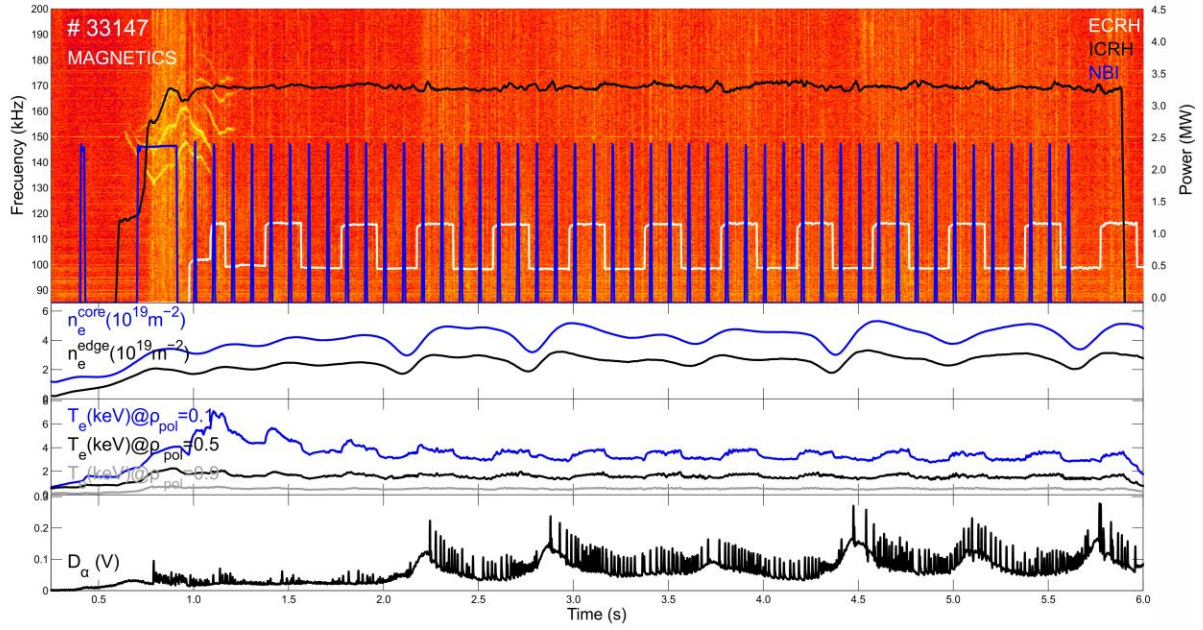Figure 6 (colour online). Phase magnetic spectrogram showing toroidal mode numbers of the excited TAEs in Figure 5.

Figure 7 (colour online). Zoom of the top box in Fig.5 showing fine time scales for TAE excitation/ disappearance with ECRH.

| Figure 8 (a) (colour online): Top: TAE mode structure computed with the spectral MISHKA code [15]; Bottom: amplitude of the same TAE as function of R and Z measured with ECEI array. Here, R=1.85 m corresponds to s≡ρ_p≈0.44, and R=1.9 m corresponds to s≡ρ_p≈0.55. | Figure 8 (b) (colour online): position of the ECEI imaging array in the AUG experiments on ECRH/TAE. |

2.2 No effect on TAE stability from ECRH applied on-axis

In contrast to discharges with ECRH applied off-axis, no effect on TAE stability was observed when ECRH was applied on-axis. Figure 9 shows magnetic spectrogram and temporal evolution of main plasma parameters in discharge #33147 with on-axis ECRH. TAEs are observed at the beginning of this discharge only, at t < 1.3 s, before the start of the modulation power wave-form of ECRH.
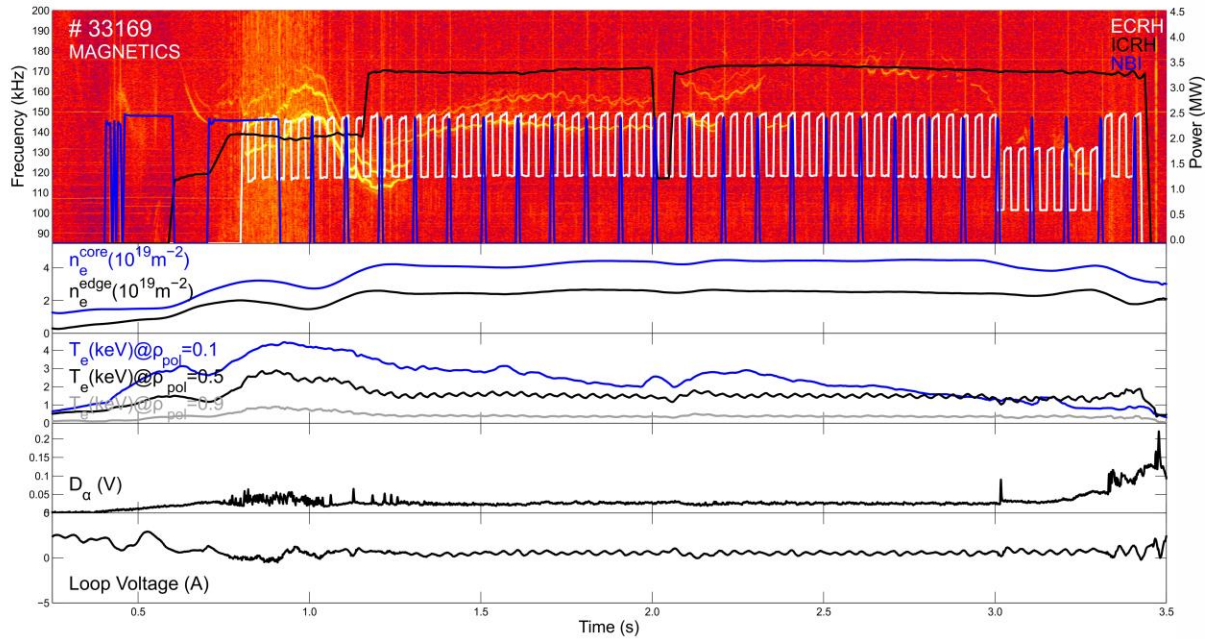

Figure 9 (colour online): From top to bottom: i) Magnetic spectrogram showing excitation of TAEs and power wave-forms of ICRH (black), ECRH (white) and NBI (blue); ii) temporal evolution of n_e on-axis and at the plasma edge, iii) temporal evolution of T_e on-axis, at half-radius, and at the plasma edge, and iv) D_α signal. AUG discharge #33147 with on-axis ECRH.

2.3 Co- and counter-current ECCD applied at $\rho_p \approx 0.6$ affect TAE frequency, but not stability

Taking into account recent demonstration of strong ECCD effects on beam-driven AEs in stellarators [16-18], a study of the effect of ECCD on TAEs has started on AUG. Although an unambiguous interpretation of the ECCD effects on AEs in stellarators is not accomplished yet, changes in the iota profile could be the main mechanism affecting AEs [18]. On AUG, four discharges were performed with co-current ECCDt applied on-axis, at ρ_p =0.3, and ρ_p =0.6, with ECRH modulation rates 200 ms/ 200 ms and 21 ms/ 21 ms. In the cases with short-period ECCD modulation, sawteeth did not appear in the discharges. One discharge (pulse #33170) was performed with counter-current ECCD applied at ρ_p =0.6 with 21 ms/ 21 ms modulation rate. The power of ECCD was deposited at the radius where the TAE mode structure was expected to be peaked, in order to maximise the effect on magnetic shear and

the mode continuum damping. However, in all cases, ECCD was found to cause a modulation of the TAE frequency, but no obvious effect on TAE stability was observed. Figure 10 shows a typical discharge with co-current ECCD applied at ρ_p =0.6. No significant difference is seen between ECCD and ECRH effects on TAEs, but more data are needed for a conclusion on the ECCD effects.

Figure 10 (colour online): From top to bottom: i) Magnetic spectrogram showing excitation of TAEs and power wave-forms of ICRH (black), ECRH (white) and NBI (blue); ii) temporal evolution of n_e on-axis and at the plasma edge, iii) temporal evolution of T_e on-axis, at half-radius, and at the plasma edge, and iv) D_α signal, v) loop voltage. AUG discharge #33169 with co-current ECCD applied at r/a=0.6.

3. Modelling of the AUG discharges

To explain the observed evolution of TAEs during ECRH/ ECCD on AUG, the following effects were considered:
   i)   Supra-thermal electrons excite TAEs;
   ii) ECRH-driven energetic ions excite TAEs;
   iii) The significant increase of T_e affects significantly both TAE damping (radiative, ion and electron Landau) and drive from ICRH ions (as slowing down time increases);
   iv) The density rise during ECRH shifts V_A into the wave-particle resonance region;
   v)   ECRH/ECCD modifies q-profile affecting continuum damping of TAE.

ECE data were investigated to answer the question on the existence of significant population of supra-thermal electrons in these discharges. No evidence was found for supra-thermal electrons. The density range of 3-4.5 x 10^{19} m^{-3} used in our discharges was too high for the supra-thermal electrons to appear, most typical densities for supra-thermal electrons on AUG are ~ 2x 10^{19} m^{-3}.

Next, the possibility of ECRH-generated fast ions was investigated from the Neutral Particle analyser (NPA) [19] measurements. No evidence was found for an ECRH-driven fast ion population in most of our discharges, apart from pulse #33151 where some minor ion population could be associated with ECRH. However, this population is only ~10% of the ICRH-driven fast ions, and is not expected to have played a role in TAE instability.

With the first two effects not playing a role, the problem of explaining the observed TAE evolution was reduced to that of computing accurately the competition between TAE drive and TAE damping in our discharges. For computing the ICRH-drive for TAE, modelling of ICRH tail was performed with the PION [20] and SELFO [21] codes followed by a drive assessment with CASTOR-K [22], HAGIS [23], and LIGKA [24] codes. To compute TAE damping effects, the linear gyrokinetic code LIGKA was employed, which provides a description of background kinetic and fast particle effects on the MHD stability in tokamaks.

3.1. ICRH modelling

Three comparison discharges, #33147 (on-axis ECRH), #33150 (ECRH @ ρ_p =0.3), and #33151 (ECRH higher power @ ρ_p =0.5) were analysed with the PION and SELFO codes. A significant ECRH effect on the fast ion energy content was found to be caused by the increase in slowing-down time of the fast ions. The cases with TAEs close to the marginal stability were of major interest, with an example of TAEs with n=5 and n=6 excited in AUG discharge #33150 at ~2.4 s. The measured plasma parameters and SELFO computed fast ion energy contents are shown in Figures 11-12 for this AUG discharge of interest.
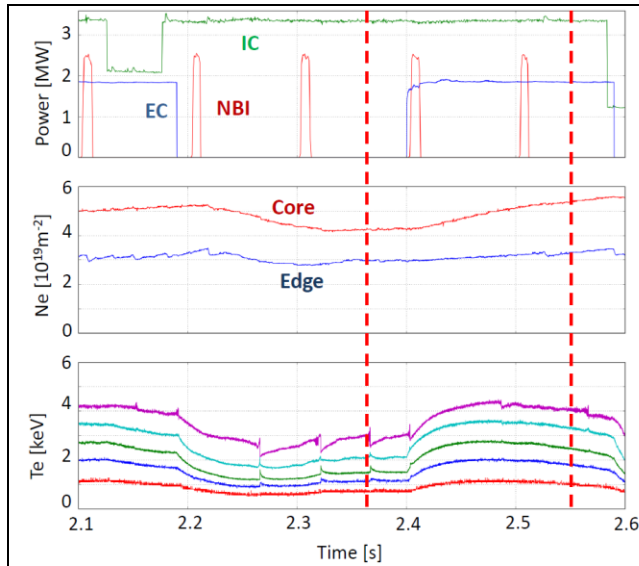

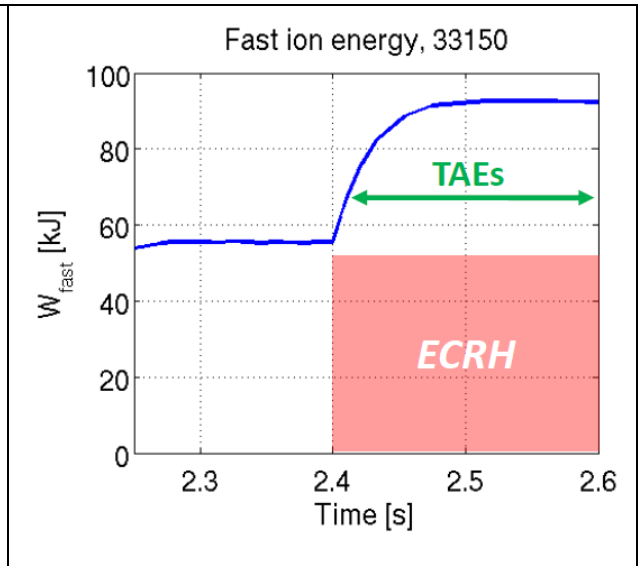| Figure 11. Top: power wave-forms of ICRH, ECRH, and NBI; Middle: plasma density evolution in the plasma core and at the edge, and Bottom: T_e evolution at different radii. The time window for the ICRH modelling is shown with two vertical broken lines. | Figure 12. Temporal evolution of the fast ion energy content in AUG pulse #33150 computed with the SELFO code. |

It is seen from the SELFO modelling that the H-minority energy contents nearly doubles when ECRH is applied at ~2.4 s and TAEs are excited. Figures 13 and 14 show the energy distribution functions and the radial fast ion pressure profiles for the near-threshold TAE-case in #33150 at around ~2.4 s.

For comparing the on-axis and off-axis ECRH effects, it was found that the ECRH effect on the shape of Te profile makes slowing-down time $\tau_{SD}(0)$ in the ECRH on-axis discharge higher than $\tau_{SD}(0)$ in the discharges with ECRH off-axis. However, $\tau_{SD}(\rho_p = 0.4)$ in the case of ECRH on-axis is significantly lower than that in the discharges with ECRH off-axis. As a result; the increase of the slowing-down time affects significantly fast ions in the ECRH off-axis discharges, and less so – in the ECRH on-axis discharges.
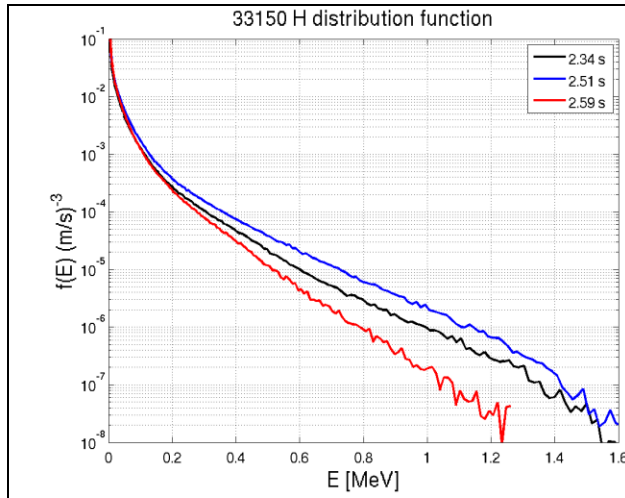

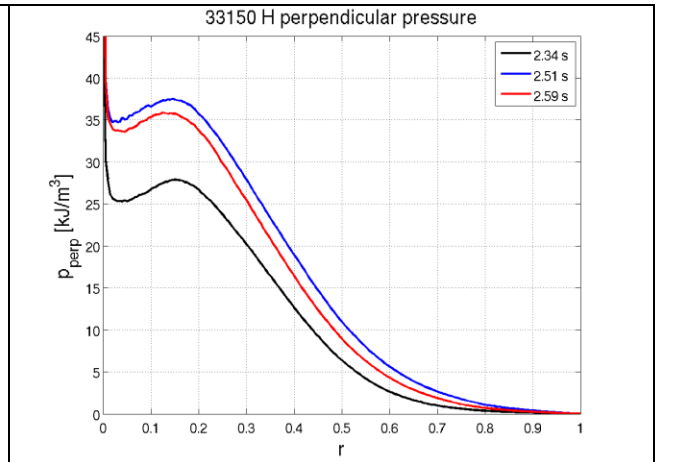| Figure 13. Energy distribution functions at different times ions computed with SELFO for fast H ions in #33150.	Figure 14. Profiles of perpendicular pressure of fast H ions computed with SELFO

3.2 Modelling of TAE drive by ICRH-accelerated ions

For the modelling of TAE drive by ICRH-accelerate ions, codes CASTOR-K, HAGIS, and LIGKA were used. Figure 15 shows plasma density, temperature, and q(r) profiles just before ECRH and just after ECRH in the discharge #33150. Deuterium plasma is considered with $Z_{eff} = 2$, with carbon impurity of $n_C/n_e = 4\%$ and tungsten impurity of $n_W/n_e = 0.05\%$. Figure 16 shows TAEs and Alfvén continua with n=5&6 computed with the LIGKA code corresponding to TAEs observed in AUG discharge #33150 at the near-threshold time ~ 2.4 s.
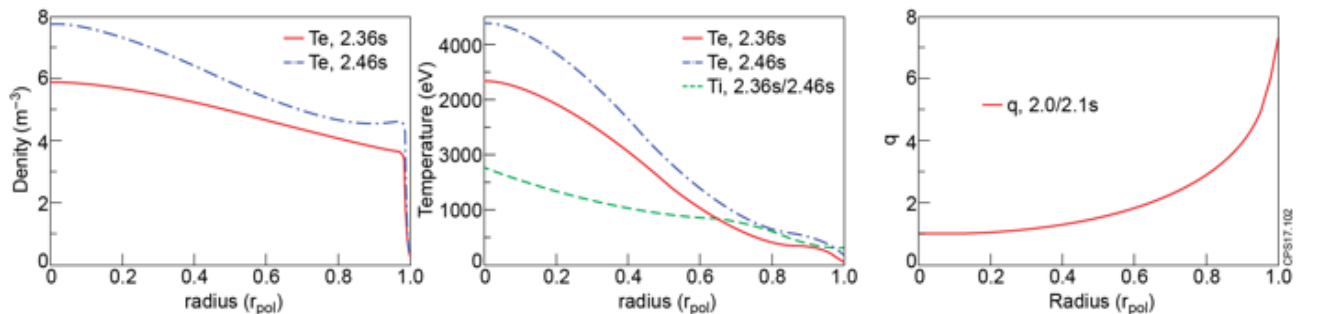
Figure 15. Left: $n_e(r)$ just before ECRH, t ~2.36 s (no TAE), and just after ECRH, t ~2.46 s (TAEs excited); Middle: $T_i(r)$ measured in #33150. Also $T_e(r)$ are shown at t ~2.36 s and t ~2.46 s; Right: q(r)- profile used in the modelling.
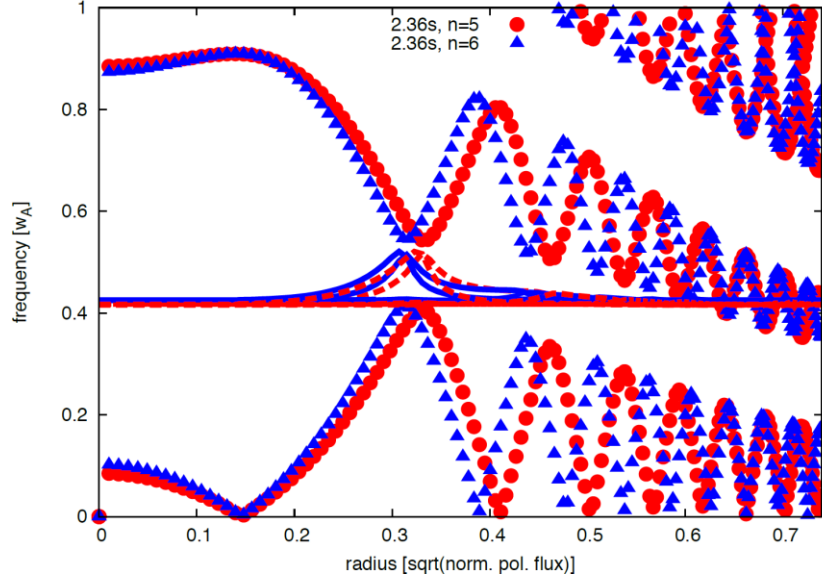

Figure 16. Core-localised TAEs with n=5 (solid blue line) and n=6 (broken red line) computed with the LIGKA code. Alfvén continua for n=5, 6 are shown with red circles and blue triangles respectively.

To assess the fast ion phase space, where the main contribution comes from the wave-particle interaction, resonance map of the contours of

$$\Omega \equiv \omega - n\omega_\phi - p\omega_\vartheta = 0 \tag{3}$$

was computed with the HAGIS and CASTOR-K codes for the on-axis ICRH with the trapped fast ion banana orbits having their turning points at $R=R_0$. Here, $\omega_\vartheta = \omega_\vartheta(E, P_\varphi, \Lambda,)$ and $\omega_\varphi = \omega_\varphi(E, P_\varphi, \Lambda)$ are the poloidal orbit frequency and the toroidal precession frequency of the fast ions, n and ω are toroidal mode number and frequency of the mode, p is the bounce harmonic, and $E = mV^2/2$, $P_\varphi = e_i\psi_p + m_iRV_\parallel(B_\varphi/B)$, $\Lambda = \mu B_0/E$ are the phase space variables describing energy, toroidal canonical momentum, and pitch-angle variable of the fast ion orbits. For the banana orbits at their turning points, $V_\parallel = 0$, and the toroidal canonical momentum depends on the poloidal flux ψ_p only, $P_\varphi = e_i\psi_p(Z)$, where e_i is the fast ion charge. Furthermore, ICRH-accelerated ions with their banana tips at the magnetic axis, $R = R_0$, have $\Lambda = 1$, and Eq.(3) describes the resonances in 2D space phase only, E, P_φ, where the canonical variable could be substituted by $Z = Z(P_\varphi)$. Figure 17 shows a plot of $1/\Omega(E, Z)$ for the range of energies and radii of the particles investigated, from which one could identify the regions of phase space where a resonant interaction gioverned by Eq.(3) could occur. It is seen that the strongest resonance with p=0 corresponds to ICRH-accelerated

trapped ions in the energy range between 200 keV and 500 keV. One can conclude therefore that optimum energy of the fast ions driving the TAEs does not require an increase in ICRH power increase or a decrease in H concentration. An assessment of the temporal evolution of the fast ion distribution following the applied ECRH off-axis shows an increase in the TAE growth rate by up to an order of magnitude depending on the TAE mode structure.
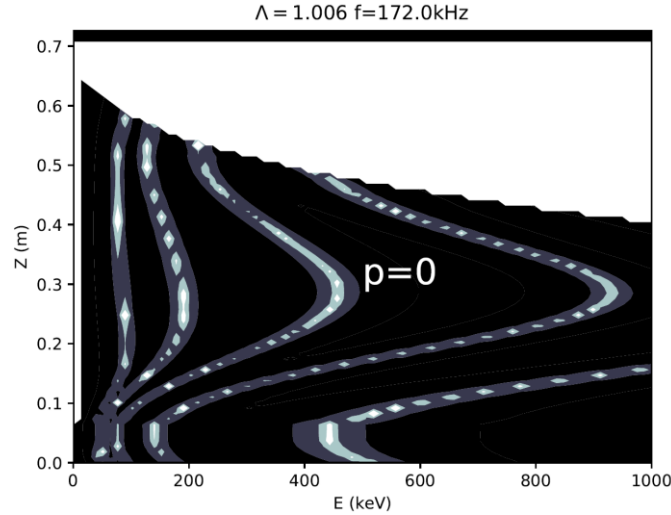

Figure 17. Resonance map for ICRH-driven TAEs in AUG discharge #33150, t~ 2.4 s

3.3 Kinetic LIGKA modelling of TAE damping effects during ECRH

Three main TAE damping mechanisms were investigated for the near-threshold TAE case in AUG discharge #3315:

i)   Continuum damping;

ii) Thermal ion Landau damping,

iii) Radiative damping.

The electron damping effects were found to be small. For the continuum damping, no significant change in the distance between TAE localisation and the continuum crossing point was found during the ECRH phase. Hence, the role of the continuum damping for the given plasmas profiles (Figure 15) was found to be negligible.

The remaining ion Landau and radiative damping effects were both found to increase significantly as T_e rises from the applied ECRH. Figure 18 summarises the LIGKA scan over T_e showing an increase in the damping rate of up to ~50%. However, the increased damping of TAEs is overcome by the additional ICRH drive due to higher W_{fast}.
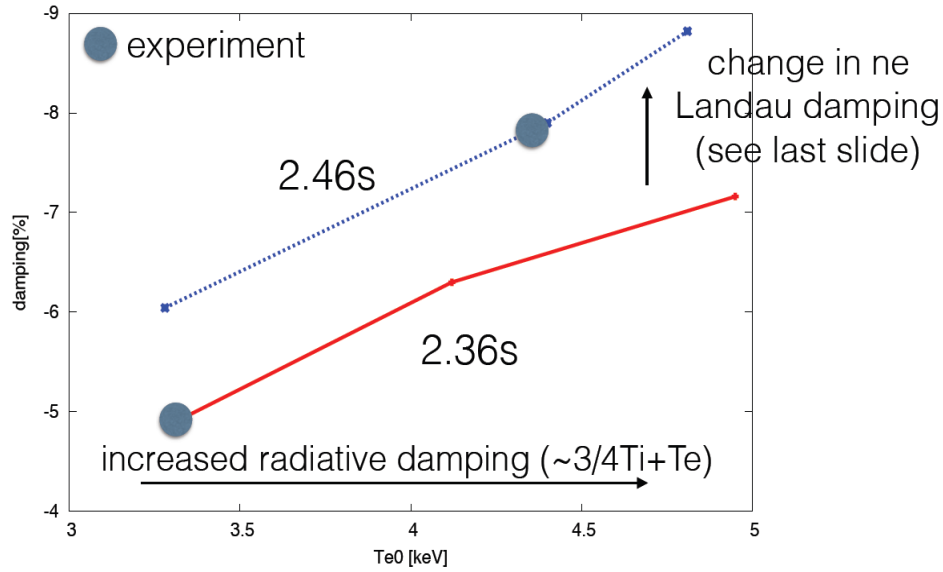
Figure 18. With ECRH applied at r/a=0.3, both ion Landau damping and radiative damping increase as shown by the LIGKA modelling.

4. Conclusions

In summary, following the discovery of the effects of ECRH on two types of Alfvén Eigenmodes, ACs and TAEs on DIII-D [3,8,9], dedicated AUG experiments were performed to investigate similar effects further. Only off-axis ECRH affects the mode stability, while ECRH on-axis had a relatively minor effect on TAE frequency only. It was established in DIII-D experiments [3, 8, 9] that ECRH mitigates ACs in shear-reversed discharges due to the increasing T_e and ∇T_e shrinking the AC frequency zone and causing high AC damping.

In the case of monotonic q(r)-profiles, off-axis ECRH was found to facilitate TAE instability on DIII-D and in dedicated AUG experiments. A significant increase in fast ion population due to the increased slowing-down time was identified as the main effect in the case of TAEs. We conclude that although ECRH effects on AE stability in present-day experiments may be quite significant, they are determined by the changes in the plasma profiles and are not particularly ECRH specific. This conclusion may be re-considered for the case of ECCD, but further investigation of ECCD effects on AEs are required to construct a statistically representative data base.

In the case of ITER, the effects of ECRH may be of importance for affecting ICRH- or NBI-driven AEs along the ITER transport path from the start of the plasma to the Q=10 scenario. On the path to the Q=10 operation, electron heating by fusion-born α-particles may be not strong enough, so that ECRH could play a role. In particular, possible effects on AEs from ECCD applied on ITER to, e.g., stabilise sawteeth or NTMs, need special investigation.

References

[1] ITER Physics Basis, Chapter 5, 1999 Nuclear Fusion 39 2471

[2] Fasoli A et al., 2007, Chapter 5 Nuclear Fusion 47 S264

[3] Van Zeeland M A et al., 2008 Plasma Phys. Control. Fusion 50 035009

[4] Garcia-Munoz M et al., 2015 IAEA TM on Energetic Particles in Magnetic Confinement Systems, IAEA HQ, Vienna, 4-7 September

[5] Hawryluk R J, An Empirical Approach to Tokamak Transport, in Physics of Plasmas Close to Thermonuclear Conditions, ed. by B. Coppi, et al., (CEC, Brussels, 1980), Vol. 1, pp. 19-46

[6] Geiger B et al., 2013 Rev Sci Instr 84 113502

[7] Berk H L et al., 2002 Phys. Rev. Lett 87 185

[8] Sharapov S E et al., 2002 Phys. Of Plasmas 9 2027

[9] Cheng C Z, Chen L, and Chance M S, 1985 Ann. Phys. 161 21

[10] Van Zeeland M A et al., 2016 Nucl Fusion 56 112007

[11] Van Zeeland M A et al., 2009 Nucl Fusion 49 065003

[12] Mlynek A et al., 2011 Nucl. Fusion 51 043002

[13] Cupido L et al., 2006 Rev Sci Instr 77 10E915

[14] Freethy S.J. et al., 2016 Rev Sci Instr 87 11E102

[15] Mikhailovskii A B et al., 1997 Plasma Phys Rep 23 844

[16] Nagaoka K et al., 2013 Nucl. Fusion 53 072004

[17] Yamamoto S 2014 Effect of ECH/ECCD on energetic-ion driven MHD instabilities in low shear helical plasmas, US-Japan JIFT meeting, Kyoto University., June 3–5

[18] Cappa A et al., 2015 Impact of ECRH on the NBI-driven Alfvén activity in the TJ-II stellarator: experiments and data analysis, 14th CWGM Warsaw

[19] Schneider P A et al., 2015 Rev Sci Instr 86 073508

[20] Eriksson L-G et al., 1993 Nucl Fusion 33 1037

[21] Hedin J et al., 2002 Nucl Fusion 42 527

[22] Borba D and Kerner W, 1999 J Comput Physics 153

[23] Pinches A D et al., 1998 Comp Physics Comm 111 133

[24] Lauber P et al., 2007 J Comput Physics 226 447